Journal of Materials Chemistry C

PAPER

View Article Online
View Journal | View Issue

Cite this: J. Mater. Chem. C, 2017, 5, 408

Zigzag double-chain C–Be nanoribbon featuring planar pentacoordinate carbons and ribbon aromaticity†

Jia-Jia Li,[a] Yuewen Mu,[a] Xinxin Tian,[a] Caixia Yuan,[a] Yan-Bo Wu,*[a] Qiang Wang,*[b] Debao Li,[b] Zhi-Xiang Wang[c] and Si-Dian Li*[a]

Received 8th October 2016,
Accepted 2nd December 2016

DOI: 10.1039/c6tc04356a

www.rsc.org/MaterialsC

Low-dimensional materials (LDMs) involving planar hypercoordinate carbon bonding were predicted to have applications in electronic devices, energy materials, and optical materials, *etc.* The majority of carbon atoms in such LDMs adopt a tetracoordinate structure, while examples with a higher coordination number are extremely rare and the bonding geometries of those carbons are not perfectly planar. In this work, we designed ribbon-like clusters $C_nBe_{3n+2}H_{2n+2}^{2+}$ with planar pentacoordinate carbons (ppCs) and extended the corresponding structural model under 1D periodic boundary conditions (PBCs), leading to a zigzag double-chain C–Be nanoribbon. The beryllium atoms in such a nanoribbon arrange in a cosine shape around the perfect ppCs, which are unprecedented in LDMs. Detailed analyses revealed that the perfect ppC structure in the nanoribbon was geometrically achieved by opening a Be–Be edge of small Be_5 rings, thereby making the intra-ring space adjustable to fit the size of the carbons. Electronically, the structure is stabilized by a favourable sandwich type charge distribution and satisfaction of the octet rule for ppCs. Note that all the valence electrons in the nanoribbon are locally delocalized within each ppC moiety, representing a new type of ribbon aromaticity, which should be useful in nanoelectronics. The nanoribbon and its cluster precursor $C_2Be_8H_6^{2+}$ are thermodynamically stable, and are promising targets for experimental realization. The nanoribbon was predicted to be an indirect band gap semiconductor; thus it has potential applications in designing light-weight electronic devices.

Introduction

Planar tetracoordinate carbon (ptC) has long fascinated chemists because of its novel structure beyond the classical tetrahedral tetracoordination of saturated carbon. The ptC structure was first proposed in a transition state in 1968 by Monkhorst.[1] In 1970, Hoffmann *et al.* compared the electronic structures of tetrahedral and planar methane and proposed strategies to stabilize ptC.[2] The first ptC minimum, 1,1-dilithiocyclopropane, was reported by Schleyer and Pople *et al.* in 1976.[3] Since then, numerous ptC species have been designed computationally or even realized experimentally.[4–10]

In addition to ptC, planar penta-, hexa-, and heptacoordinate carbons (ppC, phC, and p7C) were proven to be possible by Schleyer's group in 2000–2001.[11,12] Subsequently, a number of ppC or phC species turned out to be thermodynamically and/or kinetically stable. Examples include the ppC species $CBe_4H_4Li_2$, $CAl_nBe_m^{n-4}$ (n = 2–5, $n + m$ = 5), CBe_5E^- (E = Al, Ga, In, or Tl), $CBe_5Li_n^{n-4}$ (n = 1–5), $CBe_5H_n^{n-4}$ (n = 2–5), and $CBe_5X_5^+$ (X = F, Cl, or Br)[13–20] as well as the phC species $CO_3Li_3^+$, $CN_3Be_3^+$, and $CN_3Mg_3^+$.[21,22] They are good targets for gas phase generation and characterization. Remarkably, it can be found that beryllium often appears as the ligand atom in these stable ppC or phC species.

As an extension of small clusters, big clusters or low-dimensional materials (LDMs) with planar hypercoordinate carbons have also been extensively studied.[23–40] Some of these LDMs had been predicted to have great application potentials in fields including energy conversion materials, optical materials, and electronic devices and mechanics, *etc.*[24–34]

However, the majority of planar hypercoordinate carbons in LDMs are ptCs, whereas examples of LDMs with a higher

[a] Key Lab for Materials of Energy Conversion and Storage of Shanxi Province and Key Lab of Chemical Biology and Molecular Engineering of Ministry of Education, Institute of Molecular Science, Shanxi University, Taiyuan, Shanxi, 030006, People's Republic of China. E-mail: wyb@sxu.edu.cn, lisidian@sxu.edu.cn

[b] State Key Laboratory of Coal Conversion, Institute of Coal Chemistry, The Chinese Academy of Sciences, Taiyuan, Shanxi, 030001, People's Republic of China. E-mail: wqiang@sxicc.ac.cn

[c] School of Chemistry and Chemical Engineering, University of the Chinese Academy of Sciences, Beijing 100049, People's Republic of China

† Electronic supplementary information (ESI) available: A figure incorporating the NBO results of **3–5**, figures for the AdNDP results of **1** and **3–5**, and the Cartesian coordinates of the optimized structures of **1–5** at B3LYP/cc-pVTZ and M06-2X/cc-pVTZ levels, **1–3** at the B2PLYP-D3/cc-pVTZ level, and the low-lying isomers of **2** at the B3LYP/cc-pVTZ level. See DOI: 10.1039/c6tc04356a

number of coordination for planar carbon are extremely rare. On the one hand, planar pentagons and heptagons are topologically unsuitable for edge-shared fusion to form infinite planar structures. Furthermore, it would be too crowded for six or seven ligand atoms to distribute around the small carbon in a perfect plane. Such a situation is especially severe in LDMs due to the steric constraints. We note that the recently reported Be_5C_2 and Be_2C monolayers are unique examples of LDMs featuring ppC and phC, respectively.[41,42] The beryllium atoms are also the key ligands for the ppCs and phCs in the monolayers. Nevertheless, they are not arranged in an exact plane with the central carbons. To our knowledge, LDMs with impeccable ppC, phC, or p7C are hitherto unknown.

Geometrically, if all the vertexes of an uninterrupted planar pentagonal ring are beryllium atoms, the intra-ring spaces are often a little small for a ppC to stay at the center. The typical examples are quasi-planar rather than the perfect planar structures that are found in C_{5v} $CBe_5H_5^+$ and C_s CBe_5H_4 clusters[19] as well as Be_5C_2 and Be_2C monolayers.[41,42] Therefore, it is necessary to enlarge the intra-ring spaces to well accommodate the carbon atom at the ring center. In this work, through a strategy of opening the Be–Be edge of a Be_5 ring, we achieved enlarged intra-ring spaces as well as perfect ppCs in the ribbon-like clusters $C_nBe_{3n+2}H_{2n+2}^{2+}$ (n = 4, 5) and the corresponding $C_2Be_6H_4$ nanoribbon.

Computational details

The ribbon-like clusters were optimized and the harmonic vibrational frequencies were analyzed at the B3LYP/cc-pVTZ level. The feasibility of the B3LYP functional was calibrated by conducting M06-2X/cc-pVTZ calculations on all the ppC clusters and B2PLYP-D3/cc-pVTZ calculations on the clusters with one, two, and three ppCs, which both gave almost identical geometries to those obtained at the B3LYP/cc-pVTZ level and also identified their minima natures. Therefore, the following discussions on the cluster systems are based on the B3LYP results; we have put the M06-2X and B2PLYP-D3 results in the ESI.† Natural bond orbital (NBO)[43] analyses were performed at the B3LYP/cc-pVTZ level to understand the bonding. The aromaticity in non-classical systems may be very important for their stabilization,[44] thus nucleus-independent chemical shift (NICS)[45,46] calculations were carried out at the same level to assess the aromaticity of the non-classical clusters. Adaptive natural density partitioning (AdNDP)[47] analyses were carried out at the B3LYP/6-31G level. The ppC-containing nanoribbon under periodic boundary conditions (PBCs) was optimized at the GGA-PBE level using the projector augmented wave (PAW)[48,49] pseudopotential method with a plane wave energy cutoff of 500 eV and a 1 × 1 × 7 k-point mesh. The band structure and density of states (DOS) were calculated using a cutoff of 550 eV and a 1 × 1 × 11 k-point mesh. The potential energy surface (PES) of **2** was explored using both a stochastic search algorithm[50,51] and a particle swarming optimization (PSO)[52,53] method, with the initial optimization performed at the B3LYP/6-31G(d) level and the ten lowest isomers re-optimized and the vibrational frequencies analyzed at the B3LYP/cc-pVTZ level. The single point energies of the five lowest isomers were improved at the CCSD(T)/cc-pVTZ level based on the B3LYP/cc-pVTZ structures and corrected with B3LYP/cc-pVTZ zero-point energies. The PES of the nanoribbon under PBCs was explored using the PSO method. The initially generated structures were optimized at the PBE level with a plane wave energy cutoff of 400 eV and then reoptimized using a cutoff of 500 eV to determine the energy order. A stochastic search of the PES of $C_2Be_8H_6^{2+}$ was realized using the GXYZ program,[54,55] the AdNDP analysis was performed using the AdNDP program,[56] and the PSO exploration of the PES was carried out using CALYPSO codes.[57] The calculations considering the PBCs, except for the location of the isomers of **2**, were performed using the Vienna *ab initio* simulation package (VASP),[58,59] the CCSD(T) energies were calculated using the MolPro 2012.1 package,[60] and the other calculations were carried out using the Gaussian 09 package.[61]

Results and discussion

Our design started from the topological analyses of the plausibility of the edge-shared fusion of pentagons in a plane. Though a pentagon is unsuitable as a building block to design a two-dimensional (2D) plane *via* such fusion, it can be suitable for zero-dimensional (0D) species and one-dimensional (1D) ribbons. Given in Scheme 1 are some concise examples (**A** is 0D and **B–D** are 1D). We note that the simplest 1D model, **B**, is different from the other models in that all the pentagons in **B** are arranged in the opposite direction to the neighbouring pentagons.

Design of ppC-containing ribbon clusters and nanoribbons

Bearing the arrangement of the pentagons in model **B** in mind, we chose our previously reported species C_s CBe_5H_4 (see **1** in Fig. 1) as the building block for designing LDMs with ppCs. **1** was chosen because it is relatively easy to eliminate the steric collisions among the bridging H atoms by letting the blank edges of the pentagons locate at the bold red positions of model **B** (Scheme 1).

We first re-optimized **1** at the B3LYP/cc-pVTZ level, generating a quasi-planar structure with C_s point group symmetry. Based on the above analyses, we reasoned that a non-planar geometry should be the result of insufficient intra-ring space. Consistently, the lengths of the Be–Be edges with H atoms in **1** are close to that

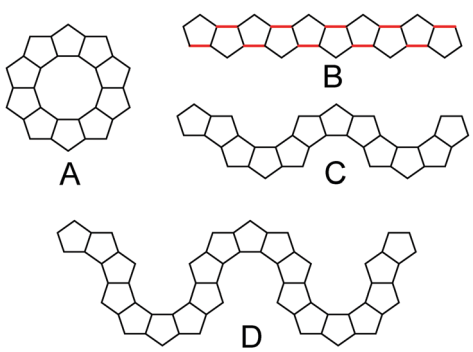

Scheme 1

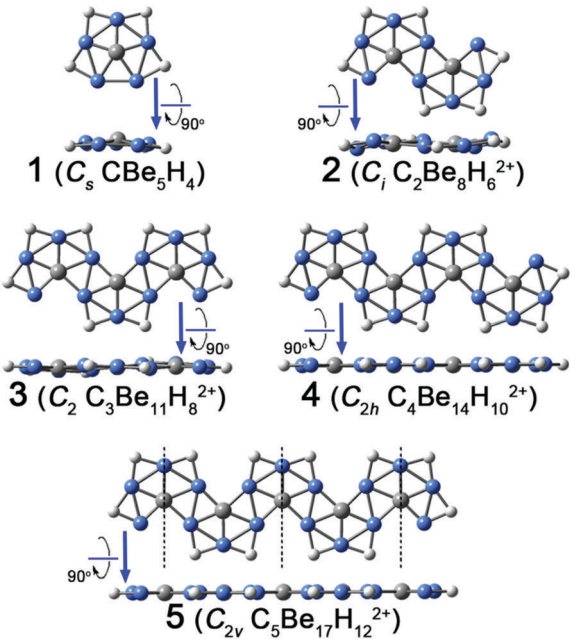

Fig. 1 Optimized structures of **1–5**. Color codes: C: grey, Be: blue, and H: white.

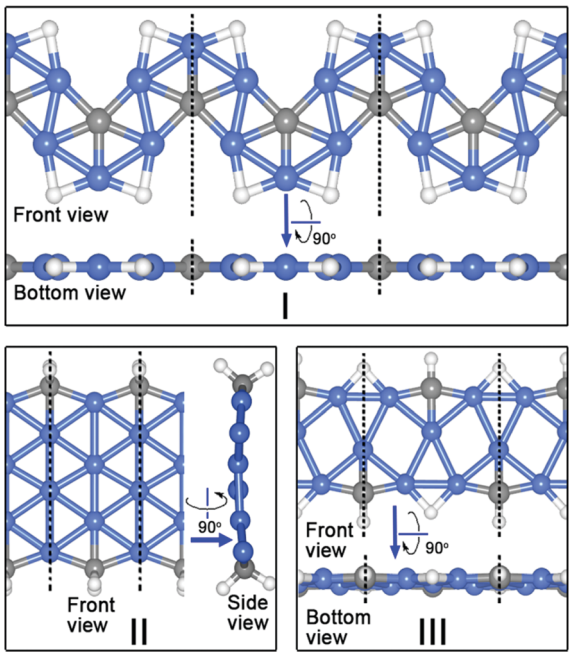

Fig. 2 The structures of the three lowest energy nanoribbons with the stoichiometry of $C_2Be_6H_4$. The dashed lines on the structures divide the different unit cells. Color codes: C: grey, Be: blue, and H: white.

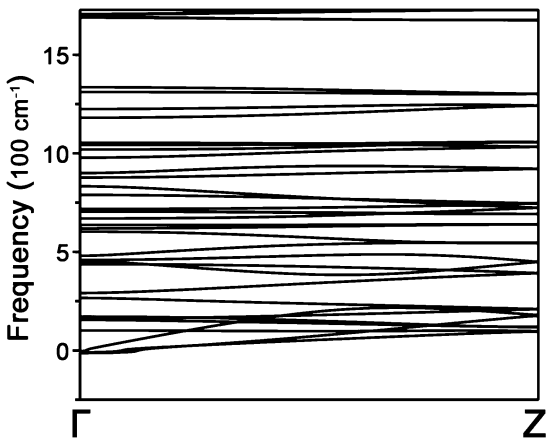

Fig. 3 Phonon spectrum of nanoribbon **I**.

without a H atom (1.921 and 1.989 Å *versus* 1.934 Å), *i.e.* the blank Be–Be edge in the Be_5 ring of **1** does not open. The situation changed when two CBe_5H_4 units were fused together in an edge-sharing manner, resulting in a dicationic species with two quasi-ppCs, *i.e.* C_i $C_2Be_8H_6^{2+}$ (see **2** in Fig. 1). Remarkably, the interatomic distance for the Be–Be edge without the H atom had elongated from 1.934 Å (in **1**) to 2.467 Å (in **2**); and the opening of such a Be–Be edge may benefit the planarization of bonding to the central carbon. Consistently, though **2** does not adopt a perfectly planar structure, both carbon atoms are located at almost the center of their peripheral five beryllium atoms (see bottom view of **2** in Fig. 1). Note that the HOMO–LUMO gap of **2** is much larger than that of **1** (4.36 *versus* 2.61 eV), indicating a more stable electronic structure in **2** than in **1**.

Obviously, the structural model in **2** could be further extended and we constructed the clusters $C_nBe_{3n+2}H_{2n+2}^{2+}$ (n = 3–5) (see **3–5** in Fig. 1) as a demonstration. At the B3LYP/cc-pVTZ level, **3** still adopted the quasi-planar structure, but the deviation of the atoms from the approximate molecular plane was noticeably smaller than that in **2**. Interestingly, the longer ribbons **4** and **5** both adopted planar geometries possessing perfect ppCs. With the elongation of the ribbon-like structures, the HOMO–LUMO gaps of the clusters showed an obviously decreasing trend (3.58, 3.07, and 2.60 eV for **3**, **4**, and **5**, respectively).

Analyzing the long ribbon-like clusters like **5**, a repeated substructure with a general formula of $C_2Be_6H_4$ can be found (see the fragments between the dashed lines on **5** in Fig. 1) and each of these units has zigzag-arranged ppC atoms. Based on such findings, we designed a nanoribbon by extending the structural models in **2–5**. As shown in Fig. 2-**I**, the nanoribbon is perfectly planar after symmetry-unrestrained geometry optimization. The phonon spectrum (see Fig. 3) also reveals an energy minimum. In such a structure, the beryllium atoms adopt an uninterrupted cosine-shaped arrangement around the isolated ppCs, which forms the novel zigzag double-chain C–Be nanoribbon. The necessary hydrogen atoms attach to the bridged positions of the Be–Be bonds at both sides of the ribbon. The nanoribbon lattice parameter (a) of **I** is 5.74 Å, which is very close to the distance between the repeated carbon atoms in **5** (~5.76 Å).

Stability of $C_2Be_8H_6^{2+}$ and $C_2Be_6H_4$ nanoribbons

Thermodynamic stability is crucial for experimental realization. Taking the ribbon precursor **2** as an example of a ribbon cluster, we studied its thermodynamic stability by extensively exploring its potential energy surface. High level *ab initio* calculations ranked **2** as the global minimum, which was 0.10 eV (2.3 kcal mol^{-1})

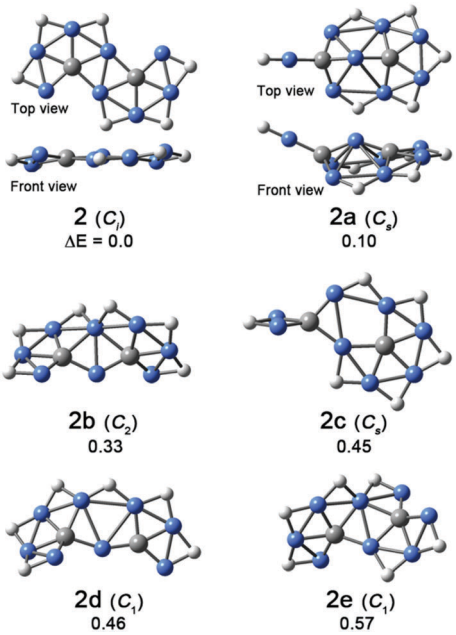

Fig. 4 B3LYP/cc-pVTZ optimized structures, their point groups, and the relative energies (ΔE, in eV) of the low-lying $C_2Be_8H_6^{2+}$ isomers. ΔE is calculated at the CCSD(T)/cc-pVTZ+B3LYP zero-point energy level and the energy of **2** is set as zero.

lower than the second lowest isomer (see **2a** in Fig. 4). Furthermore, the thermodynamic stability of nanoribbon **I** can be verified firstly by its high cohesive energy of 51.78 eV (4.32 eV per atom), and secondly, an exploration of the potential energy surface revealed that though **I** (see Fig. 2) is not competitive compared to several 2D structures, it is the lowest energy nanoribbon, with the second lowest nanoribbon (**II**, see Fig. 2) being 0.82 eV (18.8 kcal mol^{-1}) higher in energy. These results suggest that these ribbon-like structures are thermodynamically stable, which facilitates future experimental realization.

Electronic structure of ppC-containing ribbons

To understand the chemical bonding in nanoribbon **I**, we performed a deformation electronic density analysis. Compared to the atomic density, **I** has electron-accumulation regions within the CBe_5 six-center ppC moieties and the Be–H–Be three-center triangular moieties, suggesting that the chemical bonds are formed there (Fig. 5A). We also noted that neither the electron accumulation nor the electron depletion regions were distributed onto any of the Be–Be edges. Consistently, the electron localization function (ELF, see Fig. 5B) analysis of nanoribbon **I** suggests that the bonding interactions only occur in the individual CBe_5 pentagons and Be–H–Be triangles.

The highest valance band (HVB, see Fig. 5C) analysis shows that the occupied out-of-plane π electrons are localized in each CBe_5 moiety, while the lowest conductance band (LCB, see Fig. 5D) is distributed continuously along each side of the ribbon. Shown in Fig. 5E is the band structure of **I**, which indicates it is an indirect band gap semiconductor. The density of states (DOS, see Fig. 5F) of the ppC-containing nanoribbon reveals that the top of the full band and the bottom of the conduction band are both determined by the p_z components,

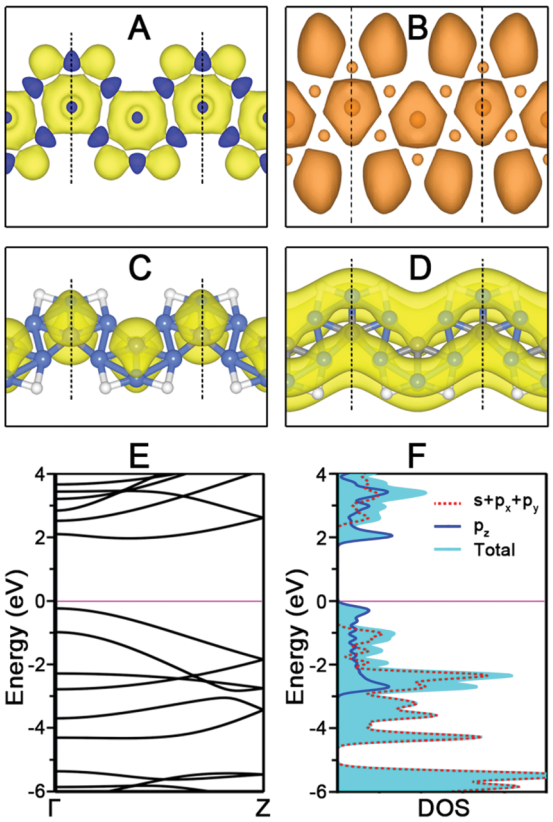

Fig. 5 Electronic structure analyses of nanoribbon **I**, including the deformation electronic density (A), the electron localization function (ELF) (B), the highest valance band (HVB) (C), the lowest conductance band (LCB) (D), the band structure (E), and the density of states (DOS) (F).

which is in accordance with the out-of-plane π character of the HVB and LCB.

To give more insight into the bonding interactions in the nanoribbon, we also analyzed the electronic structure of its cluster counterparts. The NBO results of **1** and **2** are shown in Fig. 6 and those of **3–5** are given in the ESI.† In **2**, the net charge on carbon is −1.79 $|e|$, those on the five beryllium atoms range from +0.72 to +1.18 $|e|$, and those on the peripheral hydrogen atoms range from −0.18 to −0.24 $|e|$. The charge distribution shows an efficient negative–positive–negative (− + −) sandwich-type arrangement, which is very similar to the sandwich-type charge distribution in **1** (Fig. 6) and represents a favourable type of electrostatic interaction.

The Wiberg bond indices (WBIs, see black fonts in Fig. 6) of the C–Be interactions in **2** (WBI_{C-Be}) range from 0.54 to 0.66, indicating significant covalent character and C–Be multiple center bonding. The WBI_{Be-H} values range from 0.44 to 0.48, about half of that of a single bond, suggesting the Be–H–Be three-center bonding character. Consistently, the AdNDP analyses (see Fig. 7) of **2** suggest that six of the fourteen valence electron pairs are in the Be–H–Be three-center-two-electron (3c-2e) σ bonds with occupation numbers (ONs) of 1.97–1.99 $|e|$. The remaining eight electron pairs distribute evenly into the two CBe_5 moieties, and four electron pairs in each moiety form three delocalized 6c-2e σ bonds (ONs = 1.94–1.99 $|e|$) and a

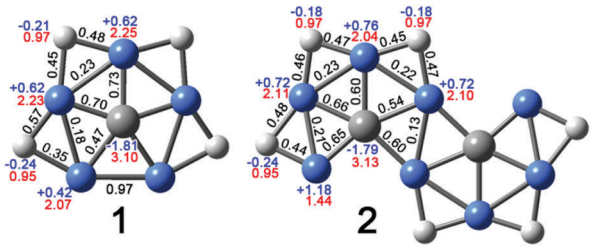

Fig. 6 The NBO results, including the Wiberg bond indices of the C–Be, Be–Be and Be–H bonds (WBI_{C-Be}, WBI_{Be-Be}, and WBI_{Be-H}, in black font), the total Wiberg bond indices of the C, Be and H atoms (WBI_C, WBI_{Be}, and WBI_H, in red font) and the natural charges (Q_C, Q_{Be}, and Q_H, in blue font) of **1** and **2** at the B3LYP/cc-pVTZ level.

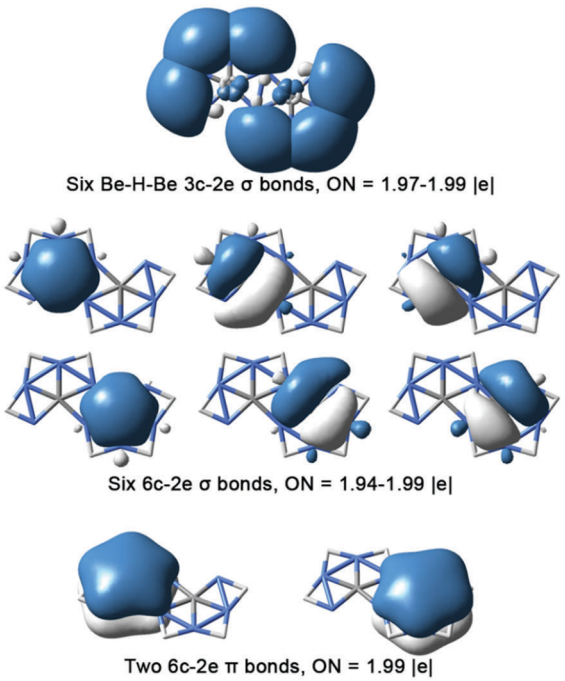

Fig. 7 The AdNDP view of chemical bonding in **2**.

delocalized 6c-2e π bond (ON = 1.99 |*e*|). Note that the delocalization of these orbitals is over the whole CBe_5 moiety including the CBe_2 triangle involved in the "opened" edge. This suggests that such Be–Be edges are only "opened" geometrically to accommodate the carbon, but are not really "opened" electronically. These delocalized orbitals support the stable eight shell electron structure around the center ppC. Markedly, no AdNDP orbitals concerning the inter-block bonding between two CBe_5 moieties can be found, which is consistent with the deformation electron density and ELF analyses of the nanoribbon **I**. We think the favourable electrostatic and covalent interactions contribute to the stabilization of **2**. The bonding interactions in **3–5** are similar to that in **2** (see Fig. S1–S5 in the ESI†), indicating similar stabilization effects.

Aromaticity

The AdNDP results also revealed six and two delocalized σ and π electrons in each CBe_5 moiety, conforming to the $4n + 2$

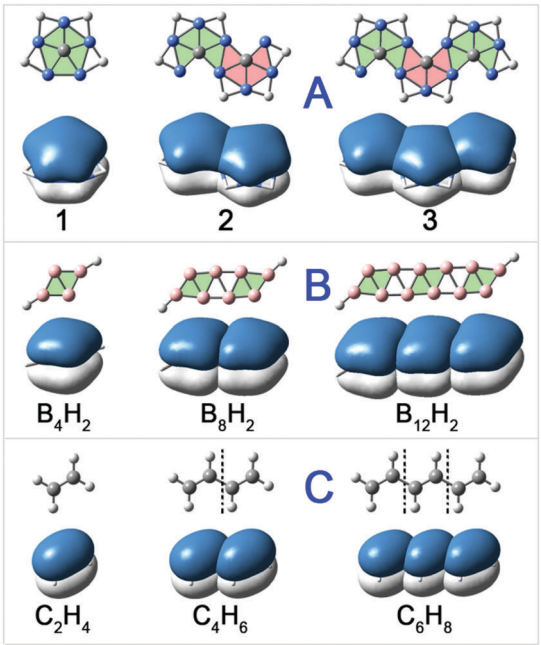

Fig. 8 The equivalent relationships of the π electron structures among zigzag double-chain C–Be ribbons, double-chain boron ribbons, and conjugated olefins.

Huckel rule with $n = 1$ and 0, respectively, and rendering σ plus π dual aromaticity to each CBe_5 moiety. Remarkably, the aromaticity in these ppC ribbons is unprecedented in that the delocalization of both the σ and π electrons is limited within the same CBe_5 moiety, revealing a new type of dual island ribbon aromaticity. Previously, we had proposed that double-chain boron ribbons (DCBRs) possessed ribbon aromaticity, but it is different from that observed in this work. In DCBRs, though there exists both delocalized 4c-2e π bonds and delocalized 4c-2e σ bonds, they are distributed alternatively in the adjacent B_4 moieties rather than in the same B_4 moiety.[62,63] Nevertheless, we note that the π electron structures of ppC-containing ribbons, DCBRs, and conjugated olefins are similar and thus an equivalent relationship between the π electron structures of these three ribbons can be established (see Fig. 8), which suggests that the ppC-containing ribbons and the DCBRs are stabilized by similar electronic structure effects to conjugated olefins.

To further characterize the aromaticity, we performed NICS analyses on planarized **2**. We examined the centers of all the Be–H–Be and Be–C–Be triangles and points up to 2 Å above these centers and above the ppC. Since the properties of the in-plane and out-of-plane regions are dominated by σ and π bonding, respectively, the NICS(0) values of −16.8 to −24.2 ppm at the centers of the Be–C–Be triangles (Fig. 9) suggested σ-aromaticity; and the values of −8.3 to −20.7 ppm at 1 Å above these centers and above the ppC (Fig. 9) indicated π-aromaticity. Therefore, the NICS analyses revealed that **2** is σ and π double aromatic, which agrees with the orbital analyses. Note that the NICS values for the CBe_2 triangle with the "opened" Be–Be edge are similar to those of the other CBe_2 triangles, revealing the CBe_5 structure to exist as a whole moiety electronically.

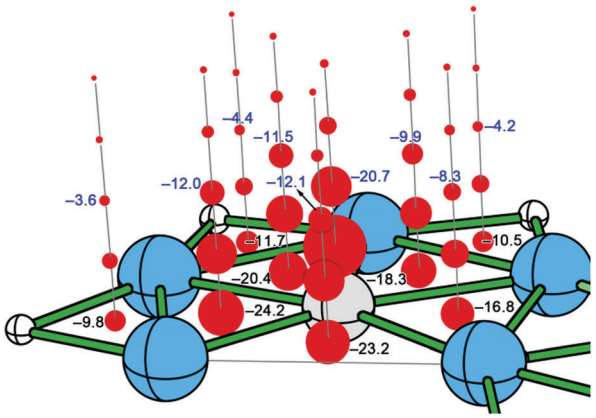

Fig. 9 The NICS values for planarized **2** at the B3LYP/cc-pVTZ level. For clarity, only the necessary part of the cluster is shown. Color code: C: grey, Be: blue, and H: white; negative NICS points: red, and positive NICS points: not applicable.

In addition to the CBe_5 moieties, each Be_2H triangle possesses a 3c-2e delocalized σ bond, revealing the σ-aromaticity. Consistently, the negative NICS(0) values of −9.8, −11.7, and −10.5 ppm at the centers (see Fig. 9) also indicate the nature of the σ-aromaticity. In contrast, as there are no π-orbitals on the Be_2H triangles, the small negative NICS(1) values of −3.6, −4.4, and −4.2 ppm may result from π-bonding in the CBe_5 moiety, so the Be–H–Be triangles are non-aromatic with regards to π-bonding. We think the aromaticity also contributes to the stabilization of the ppC-containing ribbon-like structures.

Conclusions

With the CBe_5H_4 cluster as a building block, the ribbon-like clusters $C_nBe_{3n+2}H_{2n+2}^{2+}$ (n = 2–5) were designed using the rational arrangement of CBe_5 pentagons for edge-shared fusion. Extending the structural model of these clusters under 1D periodic boundary conditions led to a thermodynamically stable zigzag double-chain C–Be nanoribbon. The carbon atoms in the nanoribbon adopt perfect planar pentacoordination, which is unprecedented in low dimensional materials. The opening of a Be–Be edge in each Be_5 ring of the nanoribbon plays a crucial role in achieving the perfect planar geometry. The favourable sandwich shape charge distribution, the satisfaction of the octet rule for ppCs, and the double aromaticity contribute to the stabilization of the ribbon-like structures electronically. The valence electrons in the ribbon structure are all locally delocalized, showing an extraordinary ribbon aromaticity, which should be useful in nanoelectronics. The nanoribbon is predicted to be an indirect band gap semiconductor; and as half of the atoms in the nanoribbon are beryllium, which is light in atomic mass, it should be useful in designing light-weight electronic devices.

Acknowledgements

The authors are grateful for the financial support of the national Natural Science Foundation of China (NSFC, Grant Nos. 21273140, 21373130, 21471092, 11504213, and U1510103), the Special Program for Applied Research on Super Computation of the NSFC-Guangdong Joint Fund (the second phase), the Program for the Innovative Talents of Higher Learning Institutions of Shanxi Province, and the high performance computer platform of Shanxi University.

References

1 H. J. Monkhorst, *Chem. Commun.*, 1968, 1111–1112.
2 R. Hoffmann, R. W. Alder and C. F. Wilcox, Jr., *J. Am. Chem. Soc.*, 1970, **92**, 4992–4993.
3 J. B. Collins, J. D. Dill, E. D. Jemmis, Y. Apeloig, P. v. R. Schleyer, R. Seeger and J. A. Pople, *J. Am. Chem. Soc.*, 1976, **98**, 5419–5427.
4 K. Sorger and P. v. R. Schleyer, *THEOCHEM*, 1995, **338**, 317–346.
5 D. Rottger and G. Erker, *Angew. Chem., Int. Ed. Engl.*, 1997, **36**, 812–827.
6 L. Radom and D. R. Rasmussen, *Pure Appl. Chem.*, 1998, **70**, 1977–1984.
7 W. Siebert and A. Gunale, *Chem. Soc. Rev.*, 1999, **28**, 367–371.
8 R. Keese, *Chem. Rev.*, 2006, **106**, 4787–4808.
9 G. Merino, M. A. Mendez-Rojas, A. Vela and T. Heine, *J. Comput. Chem.*, 2007, **28**, 362–372.
10 L. M. Yang, E. Ganz, Z. F. Chen, Z. X. Wang and P. v. R. Schleyer, *Angew. Chem., Int. Ed.*, 2015, **54**, 9468–9501.
11 Z. X. Wang and P. v. R. Schleyer, *Science*, 2001, **292**, 2465–2469.
12 K. Exner and P. v. R. Schleyer, *Science*, 2000, **290**, 1937–1940.
13 Z. X. Wang, C. G. Zhang, Z. F. Chen and P. v. R. Schleyer, *Inorg. Chem.*, 2008, **47**, 1332–1336.
14 Y. Pei, W. An, K. Ito, P. v. R. Schleyer and X. C. Zeng, *J. Am. Chem. Soc.*, 2008, **130**, 10394–10400.
15 J. O. C. Jimenez-Halla, Y. B. Wu, Z. X. Wang, R. Islas, T. Heine and G. Merino, *Chem. Commun.*, 2010, **46**, 8776–8778.
16 Y. B. Wu, Y. Duan, H. G. Lu and S. D. Li, *J. Phys. Chem. A*, 2012, **116**, 3290–3294.
17 A. C. Castro, G. Martinez-Guajardo, T. Johnson, J. M. Ugalde, Y.-B. Wu, J. M. Mercero, T. Heine, K. J. Donald and G. Merino, *Phys. Chem. Chem. Phys.*, 2012, **14**, 14764–14769.
18 R. Grande-Aztatzi, J. L. Cabellos, R. Islas, I. Infante, J. M. Mercero, A. Restrepo and G. Merino, *Phys. Chem. Chem. Phys.*, 2015, **17**, 4620–4624.
19 J. C. Guo, G. M. Ren, C. Q. Miao, W. J. Tian, Y. B. Wu and X. T. Wang, *J. Phys. Chem. A*, 2015, **119**, 13101–13106.
20 J. C. Guo, W. J. Tian, Y. J. Wang, X. F. Zhao, Y. B. Wu, H. J. Zhai and S. D. Li, *J. Chem. Phys.*, 2016, **144**, 244303.
21 Y.-B. Wu, Y. Duan, G. Lu, H.-G. Lu, P. Yang, P. v. R. Schleyer, G. Merino, R. Islas and Z.-X. Wang, *Phys. Chem. Chem. Phys.*, 2012, **14**, 14760–14763.
22 C. F. Zhang, S. J. Han, Y. B. Wu, H. G. Lu and G. Lu, *J. Phys. Chem. A*, 2014, **118**, 3319–3325.
23 P. D. Pancharatna, M. A. Mendez-Rojas, G. Merino, A. Vela and R. Hoffmann, *J. Am. Chem. Soc.*, 2004, **126**, 15309–15315.
24 X. J. Wu, Y. Pei and X. C. Zeng, *Nano Lett.*, 2009, **9**, 1577–1582.

25 M. H. Wu, Y. Pei and X. C. Zeng, *J. Am. Chem. Soc.*, 2010, **132**, 5554–5555.
26 Y. F. Li, F. Y. Li, Z. Zhou and Z. F. Chen, *J. Am. Chem. Soc.*, 2011, **133**, 900–908.
27 B. Xiao, Y. H. Ding and C. C. Sun, *Phys. Chem. Chem. Phys.*, 2011, **13**, 2732–2737.
28 G. L. Chai, C. S. Lin and W. D. Cheng, *J. Mater. Chem.*, 2012, **22**, 11303–11309.
29 M. H. Wu, Y. Pei, J. Dai, H. Li and X. C. Zeng, *J. Phys. Chem. C*, 2012, **116**, 11378–11385.
30 J. Dai, X. J. Wu, J. L. Yang and X. C. Zeng, *J. Phys. Chem. Lett.*, 2014, **5**, 2058–2065.
31 Y. F. Li, Y. L. Liao, P. v. R. Schleyer and Z. F. Chen, *Nanoscale*, 2014, **6**, 10784–10791.
32 L. M. Yang, V. Bacic, I. A. Popov, A. I. Boldyrev, T. Heine, T. Frauenheim and E. Ganz, *J. Am. Chem. Soc.*, 2015, **137**, 2757–2762.
33 B. Xiao, J. B. Cheng, Z. B. Liu, Q. Z. Li, W. Z. Li, X. Yang and X. F. Yu, *RSC Adv.*, 2015, **5**, 73945–73950.
34 X. Wang, Q. Wang, C. Yuan, X. F. Zhao, J. J. Li, D. Li, Y. B. Wu and X. Wang, *Phys. Chem. Chem. Phys.*, 2016, **18**, 11942–11950.
35 Y. B. Wu, J. L. Jiang, R. W. Zhang and Z. X. Wang, *Chem. – Eur. J.*, 2010, **16**, 1271–1280.
36 X. F. Zhao, H. X. Li, C. X. Yuan, Y. Q. Li, Y. B. Wu and Z. X. Wang, *J. Comput. Chem.*, 2016, **37**, 261–269.
37 Y. B. Wu, J. L. Jiang, H. Li, Z. F. Chen and Z. X. Wang, *Phys. Chem. Chem. Phys.*, 2010, **12**, 58–61.
38 Y. B. Wu, Z. X. Li, X. H. Pu and Z. X. Wang, *J. Phys. Chem. C*, 2011, **115**, 13187–13192.
39 Y. B. Wu, Z. X. Li, X. H. Pu and Z. X. Wang, *Comput. Theor. Chem.*, 2012, **992**, 78–83.
40 X. F. Zhao, C. X. Yuan, X. Wang, J. J. Li, Y. B. Wu and X. T. Wang, *J. Comput. Chem.*, 2016, **37**, 296–303.
41 Y. Wang, F. Li, Y. F. Li and Z. F. Chen, *Nat. Commun.*, 2016, **7**, 11488.
42 Y. F. Li, Y. L. Liao and Z. F. Chen, *Angew. Chem., Int. Ed.*, 2014, **53**, 7248–7252.
43 A. E. Reed, L. A. Curtiss and F. Weinhold, *Chem. Rev.*, 1988, **88**, 899–926.
44 J. M. Mercero, A. I. Boldyrev, G. Merino and J. M. Ugalde, *Chem. Soc. Rev.*, 2015, **44**, 6519–6534.
45 P. v. R. Schleyer, C. Maerker, A. Dransfeld, H.-J. Jiao and N. J. R. E. Hommes, *J. Am. Chem. Soc.*, 1996, **118**, 6317–6318.
46 Z. F. Chen, C. S. Wannere, C. Corminboeuf, R. Puchta and P. v. R. Schleyer, *Chem. Rev.*, 2005, **105**, 3842–3888.
47 D. Y. Zubarev and A. I. Boldyrev, *Phys. Chem. Chem. Phys.*, 2008, **10**, 5207–5217.
48 P. E. Blochl, *Phys. Rev. B: Condens. Matter Mater. Phys.*, 1994, **50**, 17953–17979.
49 G. Kresse and D. Joubert, *Phys. Rev. B: Condens. Matter Mater. Phys.*, 1999, **59**, 1758–1775.
50 M. Saunders, *J. Comput. Chem.*, 2004, **25**, 621–626.
51 P. P. Bera, K. W. Sattelmeyer, M. Saunders, H. F. Schaefer and P. v. R. Schleyer, *J. Phys. Chem. A*, 2006, **110**, 4287–4290.
52 Y. C. Wang, J. A. Lv, L. Zhu and Y. M. Ma, *Phys. Rev. B: Condens. Matter Mater. Phys.*, 2010, **82**, 094116.
53 Y. C. Wang, J. Lv, L. Zhu and Y. M. Ma, *Comput. Phys. Commun.*, 2012, **183**, 2063–2070.
54 H. G. Lu and Y. B. Wu, *GXYZ 2.0, A Random Search Program*, Shanxi University, Taiyuan, 2015.
55 Y. B. Wu, H. G. Lu, S. D. Li and Z. X. Wang, *J. Phys. Chem. A*, 2009, **113**, 3395–3402.
56 The AdNDP program was downloaded at http://ion.chem.usu.edu/~boldyrev/adndp.php.
57 The CALYPSO program was applied at http://www.calypso.cn/.
58 G. Kresse and J. Furthmuller, *Phys. Rev. B: Condens. Matter Mater. Phys.*, 1996, **54**, 11169–11186.
59 G. Kresse and J. Hafner, *J. Phys.: Condens. Matter*, 1994, **6**, 8245–8257.
60 H.-J. Werner, *et al.*, *MOLPRO 2012.1*, University College Cardiff Consultants Limited, Cardiff U.K., 2012. See ESI† for the full form of this reference.
61 M. J. Frisch, *et al.*, *Gaussian 09 Revision D.01*, Gaussian Inc., Wallingford CT, 2013. See the ESI† for the full form of this reference.
62 D. Z. Li, Q. Chen, Y. B. Wu, H. G. Lu and S. D. Li, *Phys. Chem. Chem. Phys.*, 2012, **14**, 14769–14774.
63 H. Bai, Q. Chen, C. Q. Miao, Y. W. Mu, Y. B. Wu, H. G. Lu, H. J. Zhai and S. D. Li, *Phys. Chem. Chem. Phys.*, 2013, **15**, 18872–18880.

